JCTC Journal of Chemical Theory and Computation

Article

pubs.acs.org/JCTC

Modeling Transition Metal Reactions with Range-Separated Functionals

Michael Seth,[†] Tom Ziegler,*[,†] Marc Steinmetz,[‡] and Stefan Grimme[‡]

[†]Department of Chemistry, University of Calgary, University Drive 2500, Calgary, AB T2N-1N4, Canada

[‡]Mulliken Center for Theoretical Chemistry, Institute for Physical and Theoretical Chemistry, Universität Bonn, Beringstrasse 4, D-53115 Bonn, Germany

Supporting Information

ABSTRACT: The performance of range-separated functionals for the calculation of reaction profiles of organometallic compounds is considered. Sets of high-level computational results are used as reference data for the most part. The benchmark data include a number of reactions involving small molecules reacting with the Pd atom, $PdCl^-$, $PdCl_2$, and a Ni atom, the reaction of a model Grubbs catalyst, and the ligand binding in a real Grubbs catalyst. Range-separated functionals are found to improve upon most standard local functionals especially if an optimized range-separation parameter is used. They do not represent an improvement upon the better-performed global hybrid functionals or a local functional that includes a larger number of adjustable parameters. Some unusual results for molecule−molecule interaction energies are observed and explained by a detailed analysis of the contributions to the bonding energies. The influence of range separation on the barriers and reaction energies is also investigated.

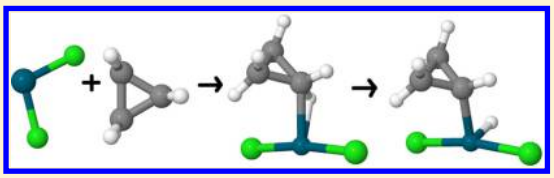

1. INTRODUCTION

Over the last thirty years or so, density functional theory has become the method of choice for most electronic structure calculations of molecules and solids in large part because of the tremendous progress that has been made in the accuracy of the developed functionals. Since there are no known procedures that guarantee that a proposed functional will improve upon known functionals, advancements have generally consisted of creating functionals that are more and more flexible in their form and then determining which components are most important for producing overall good performance. Starting from the local density approximation (LDA) where the energy density of a functional only depends on the density at the specified point in space, the natural direction of improvement was to add a dependence on the gradient of the electron density leading to the generalized gradient approximation (GGA). GGAs lead to significant improvements over LDA functionals in a number of areas. The obvious next step was to include a dependence on the second derivative of the density (or, equivalently, the kinetic energy density) resulting in meta-GGAs. The enhancements obtained were not dramatic however. A more profitable approach was found by moving in a different direction and adding a portion of nonlocal Hartree−Fock (HF) exchange (we shall also use the term "exact exchange" interchangeably with HF exchange here) to the functional.[1−3] The resulting hybrid GGAs and meta-GGAs have become the most popular functionals in use today.

These hybrid functionals can be described as "global" in the sense that they take a constant ratio of GGA/meta-GGA to exact exchange at all points in space. In the past few years there has been a number of attempts to increase the flexibility of this description to further improve the quality of functionals.

One such approach makes the admixture of DFT and exact exchange dependent on the interelectronic distance $|\vec{r}_1 - \vec{r}_2| = r_{12}$.[4−21] In practical terms, this is achieved by splitting the Coulomb operator into pieces and having one piece employed in the evaluation of the HF exchange and one piece used in the evaluation of the DFT exchange. For example, the DFT exchange may be evaluated with a Coulomb operator that is unchanged for small values of r_{12} (short-range) but is progressively attenuated as r_{12} increases (long-range) while the exact exchange is evaluated with the complementary operator that has the reverse behavior.[5,8] This type of division is one of the most commonly applied. Other partitions investigated include the opposite of that just discussed where the DFT (HF) Coulomb operator now is unattenuated at large (small) values of r_{12} and then attenuated as r_{12} decreases (increases).[12,13] More general examples exist where the DFT portion of the Coulomb operator is dominant for one extreme value of r_{12} and the HF portion is dominant at the other extreme. However, rather than going to zero the attenuating function now goes to a finite value at one or both of the extremes leading to only partial attenuation at those extremes. Even more sophisticated divisions have been proposed where the Coulomb operator is divided into more than two regions, such as the functional proposed by Scuseria and co-workers where the DFT exchange dominates for large and small values of r_{12} and exact exchange for intermediate values of r_{12} (medium range).[22]

A general functional form that can describe all of these possibilities is

Received: December 20, 2012
Published: March 19, 2013

$$\frac{1}{r_{12}} = \mathrm{DFT} + \mathrm{HF} = \frac{\alpha + \sum_i \beta_i w_i(\gamma_i, r_{12})}{r_{12}} + \frac{\delta + \sum_j \varepsilon_j w_j(\gamma_j, r_{12})}{r_{12}} \quad (1)$$

where w is a switching function that smoothly varies from 0 to 1. Further, α, β_i, δ, and ε_j are constants and γ is an attenuation parameter that controls how quickly the interaction is turned on (off). The exact form of the switching function w is typically determined by computational convenience. The error function is particularly appropriate for use with Gaussian basis functions while we have found that a good choice for an attenuating function for Slater-type basis sets is the exponential function. We should note that exponential attenuating functions have also been used in combination with Gaussian basis sets by Tenno and co-workers.[19,20] If the scaling functions w_i are exponentials then eq 1 describes a summation of scaled Coulomb and Yukawa potentials. We further note that when all of the β_i and ε_j are zero then eq 1 describes a global hybrid.

By partitioning, the Coulomb operator according to eq 1 exchange can be thought of as being divided into different ranges (short-range, long-range, and perhaps medium range) and we shall describe this type of functional as "range-separated" functionals (RS-functionals). The particular case where the DFT is fully attenuated at long-range are often called long-range corrected functionals (LC-functionals), and we shall also use this terminology if it is in common use for a given functional.

In addition to providing a more flexible method for introducing an admixture of exact exchange into a functional, RS-functionals have been proposed for a number of theoretical reasons. Early RS-functionals, where the correlation function was attenuated, were proposed in order to alleviate the difficulties associated with describing the electron cusp, thereby speeding up the convergence of wave function-based correlation methods such as configuration interaction with respect to basis set size.[7] RS-functionals where the exact exchange has been attenuated at the long (and perhaps short) range were introduced for the description of solid systems where the long-range part of the exact exchange can be troublesome to evaluate.[12,13] Conversely, LC-type functionals have been justified on the grounds that they eliminate self-interaction from a functional for long-range interactions helping to significantly improve predicted properties that can be thought of as "long-range" such as charge transfer excitations and polarizabilities.

Range-separated functionals have been shown to improve upon global hybrids in a number of areas.[14,16,23−32] Early studies aimed at predicting molecular properties found that functionals that performed well for one set of data such as thermodynamic properties did not perform well for other properties such as charge-transfer excitation energies. This lead to purpose-built RS-functionals with attenuation parameters specially optimized for a certain set of properties. More recently, LC-type functionals that retain a significant portion of short-range exact exchange have been created that seem to be more universal, at least in the case of molecules.[21,28]

We are particularly interested in the study of organometallic compounds and their use in homogeneous catalysis. DFT has provided considerable insight into the operation of transition metal catalysts.[33,34] Studied reactions of this type require the investigation of the structures and energies of reactants, products, intermediates, and transition states along the full reaction profile.

A number of studies have considered the performance of range-separated functionals for the prediction of reaction barriers.[14,16,25−32,35−38] Standard GGA functionals typically underestimate reaction barriers, especially reactions that can be classified as atom transfer reactions. Global hybrids improve on these barriers, though they often require a relatively large mixture of exact exchange. Range separated functionals have also been found to improve reaction barriers.[14,16,25−32,35−38] Truhlar and co-workers and Scuseria and co-workers have considered range-separated functionals in the study of transition metals.[21,35,39] Bond enthalpies and molecular structures were considered but a lack of suitable reference data precluded an extensive study of reaction barriers.

In this investigation, we propose to fill this gap. We will make use of two sets of benchmark results in order to assess the accuracy of range-separated functionals in the study of transition metal reactions. The nature of organometallic reactions makes the comparison between computational and experimental data challenging. High level wave function calculations are a better source of benchmark data. We therefore take our benchmark results from calculations of this type. The first set of data consist of coupled cluster results for 41 reactions studied very recently by Steinmetz and Grimme.[40] The second data set is the reaction profile of the Grubbs metathesis reaction of a model catalyst provided by Zhao and Truhlar.[41] In addition, we also consider the phosphine dissociation energy of a real model catalyst. The reference data in this case is from experiment but it is a system of interest because it has been found that many commonly used functionals do a poor job of predicting this energy[41−44]

2. COMPUTATIONAL DETAILS

All calculations were performed employing a development version of the ADF program[45−50] that includes our implementation of RS-functionals using a Yukawa potential in combination with Slater-type functions.[51]

2.1. Functionals. A number of standard functionals were employed in this study to provide data for comparison with the results obtained with RS-functionals. These functionals include GGAs BP,[52,53] BLYP,[52,54] and PBE,[55] meta-GGAs TPSS[56,57] and M06-L,[41,58] hybrids B3LYP[3] and PBE0,[59,60] and meta-hybrids TPSSh[56,57] and M06.[41,58]

RS-functionals were formed following the procedure outlined in our earlier publication.[51] An exponential function was used to attenuate the Coulomb potential in the calculation of the exact or DFT exchange. The attenuated exchange functional was obtained following the process developed for GGAs by Hirao and co-workers.[8] This procedure can be extended easily for meta-GGAs. Five range-separated functionals were formed from the GGAs and meta-GGAs considered here. The range-separation was of the LC (long-range corrected) type where for DFT the potential is attenuated for large values of r_{12} and for exact exchange it is attenuated for small values of r_{12}. This corresponds to $\beta_1 = \delta = 1$, $\varepsilon_1 = -1$, and all other parameters set to zero in eq 1. A sixth range-separated functional is the Yukawa potential analogue of the CAM-B3LYP functional (CAMY-B3LYP) where the DFT and HF potentials are attenuated as in the LC case but the attenuation functions do not go to zero or one at the extreme values of r_{12}. The parameters used are those derived by Ten-no and co-workers.[19] In the standard notation of the original CAM-B3LYP functional, they are $\alpha = 0.19$ and β

= 0.46. The equivalent parameters from eq 1 are $\alpha = 0.35$, $\beta_1 = 0.46$, $\delta = 0.65$, and $\varepsilon_1 = -0.46$. A variety of attenuation parameters (γ) were considered and the influence of this parameter will be discussed in detail in section 3.

2.2. Basis Sets and Integration Parameters. Initial test calculations utilized a valence triple-ζ basis set augmented by two polarization functions (TZ2P). This basis set was found to be satisfactory for the most part but calculated binding energies of the Ni atom to small molecules were much too high indicating an unacceptably large basis-set superposition error (BSSE). A larger quadruple-ζ basis set augmented by four polarization functions (QZ4P) was employed and demonstrated to have minimal BSSE in the Ni binding energies. Further tests found that the QZ4P basis was only required for the Ni atom and a TZ2P basis could be used for the lighter atoms in the Ni-small molecule reactions. However, it was decided to use the large QZ4P basis set for all atoms in the set of calculations dealing with the Steinmetz and Grimme database and the water dimer to eliminate any significant basis set errors. The QZ4P basis set is too large for general use and we therefore returned to the more widely applicable TZ2P basis set for the calculations involving the model and real Grubbs catalysts. The two polarization functions of the TZ2P basis set consist of a pd set for H, a df set for all main group elements, and a pf set for all transition metals. The QZ4P basis set polarization functions consist of a 2p2d set for H, a 2d2f set for second row main group elements, a 3d2f set for heavier main group elements, and a 2p3f set for transition metals. All electrons were allowed to relax in the self-consistent field calculations.

Most of the calculations utilized the standard te Velde integration grids that are the main integration workhorse in the ADF program.[61] The integration parameter for these grids was chosen to be 5. It has been found that some of the more recent Minnesota functionals can show significant errors when used in combination with standard integration grids[62] including te Velde grids.[63] Recently, the Becke grid[52] has been implemented in ADF to alleviate this problem.[63] We therefore made use of the Becke grid for all M06, M06-L, and LC-M06-L calculations. This grid type was found to give numerically stable and well-converged results even using grid parameters that correspond to intermediate fineness.

Scalar relativistic effects were included in almost all calculations through the spin-free form of the zeroth-order regularized approximation (ZORA).[64−66] The exception are the small molecule-Ni calculations where relativity was not included in order to remain consistent with the benchmark CCSD(T) results.[40]

2.3. Benchmark Data. Experimental data suitable to be used as benchmarks for theoretical predictions of transition metal reaction profiles are difficult to come by. Transition metal reactions most often take place in solution and involve molecules with a significant number of atoms. A correct description of a reaction involving large molecules in a solvent at a finite temperature requires the consideration of a number of subtle effects making comparison between theory and experiment challenging.

We therefore use for the most part high-level wave function results as our benchmark data. It is then much more straightforward to make direct comparisons between our results and the reference data. We have chosen two sets of results from the literature.

The first is the set of CCSD(T) results for a number of small-molecule reactions involving a Pd atom, $PdCl^-$, $PdCl_2$, and a Ni atom produced recently by some of us.[40] This data set consists of 13, 10, 9, and 9 reactions for Pd, $PdCl^-$, $PdCl_2$, and Ni respectively and builds upon smaller test sets investigated by Bickelhaupt[67−71] and co-workers and Martin and co-workers.[72] The reactions involve relatively small molecules from H_2 up to benzene reacting with the metal catalyst. Each reaction can be considered as taking place in two elementary steps (See Figure 1). The first step is an association reaction where the two

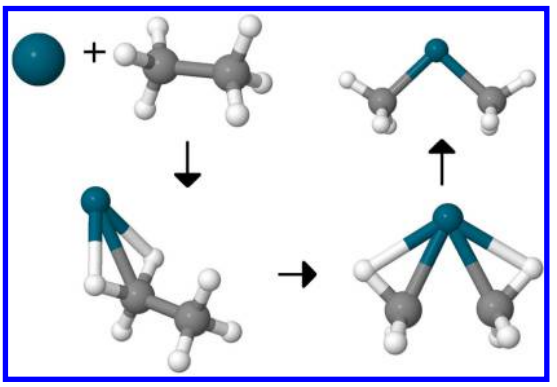

Figure 1. Example from the database of small molecule with small metal catalyst reactions involving Pd and ethane. The reaction involves reactants (top left), an initial complex (bottom left), a transition state (bottom right), and products (top right).

molecules come together to form a complex. The first step is expected to be barrierless or nearly so in all cases. All bond breaking and making takes place in the second step. Most of the second reaction steps can be considered as insertion reactions where the metal atom or molecule inserts into one of the bonds of the reacting molecule forming two new light atom-metal bonds. The exception is the S_N2 reaction of Pd with CH_3Cl where a single metal-light atom bond is formed and one light atom-light atom bond is broken. The second steps in all reactions will have non-negligible barriers on the potential energy surface.

The second set of reference data is from the study of a model Grubbs reaction performed by Zhao and Truhlar.[73] Zhao and Truhlar utilized a composite approach to estimate the large-basis set CCSD(T) energies of all stationairy points on the reaction profile of the model Grubbs catalyst $[(PH_3)(C_3H_6H_2)\text{-}Cl_2Ru{=}CH_2]$ (see Figure 2). The notation applied to describe this reaction follows that used by Zhao and Truhlar.[73]

In addition to the two sets of computational results we also compare with an experimental result that was included in the earlier study of the Grubbs reaction.[73] Here Zhao and Truhlar consider the experimental binding energy of a tricyclohexyl phosphine ligand to the metal center in a real Grubbs catalyst. We include this additional example here because the energy is predicted very poorly by many standard functionals.[42,44,73] We therefore also investigate how range-separated functionals perform when attempting to predict this energy.

As we shall see, it was found necessary to also consider the water dimer in some detail. The reference data for this system was taken from ref 74.

Geometries and energies were taken from the cited papers in all cases.

Ambiguity can arise in benchmark studies considering reaction profiles because in general the energies to be calculated

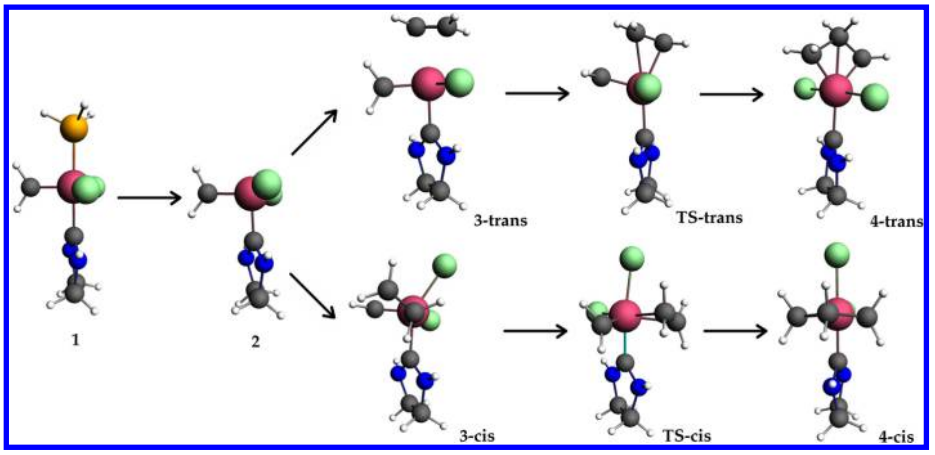

Figure 2. Stationary points along reaction path of model Grubbs catalyst.

can be defined in more than one way. For instance, if we consider reactions of the type that are present in the test set obtained by Steinmetz and Grimme a sketch of the benchmark potential energy curve is given by the black line in Figure 3.

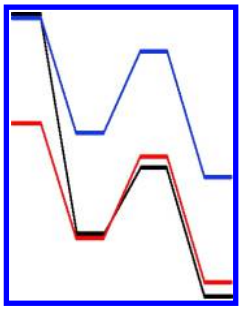

Figure 3. Benchmark reaction profile (black) compared to the same approximate profile with two different zero points (red and blue).

Also presented in Figure 3 are two different possible definitions of the calculated energies of the reaction profile (blue and red lines). The two approximate curves in red and blue come from the same results but only differ in which step in the reaction is chosen as the zero point. The reaction energies derived from the blue curve will obviously show larger average errors than those from the red curve despite the fact that they differ only in reference the point. It is not always possible to eliminate this problem entirely, and it must be kept in mind when considering statistical analyses such as those presented here.

3. RESULTS AND DISCUSSION

3.1. Small Molecule Reactions with Pd, $PdCl^-$, $PdCl_2$, and Ni. These sets of reactions, described in detail in ref 40 provide a useful benchmark set for testing the performance of a variety of functionals when describing transition-metal reactions. In their study Steinmetz and Grimme made a number of observations concerning the calculation of these

Table 1. Analysis of Calculated Reaction Energies of the Pd Atom As Compared to CCSD(T) Results[a]

		binding		$\Delta E^{\dagger}$		ΔE		total
	γ	MSD[b]	MAD[c]	MSD[b]	MAD[c]	MSD[b]	MAD[c]	MAD[c]
BP		2.1	2.1	−4.6	4.6	−5.1	5.1	3.9
BLYP		−3.5	3.5	−4.0	4.0	−5.5	5.5	4.4
PBE		3.1	3.1	−4.4	4.4	−4.4	4.4	4.0
TPSS		−0.3	2.1	−3.5	3.9	−4.3	4.5	3.5
M06-L		−1.5	1.6	0.0	2.7	0.3	2.1	2.1
B3LYP		−6.8	6.8	−0.2	1.7	−0.7	0.9	3.1
PBE0		−2.9	2.9	0.4	1.0	1.4	1.4	1.8
TPSSh		−2.7	2.8	−1.7	2.7	−2.1	2.6	2.7
M06		−5.6	5.6	3.1	3.6	6.2	6.2	5.2
LC-BP	0.75	0.9	1.3	3.9	3.9	6.8	6.8	4.0
LC-BP	0.60	3.7	3.7	2.2	2.2	4.7	4.7	3.5
LC-BLYP	0.75	−4.5	4.5	4.7	4.7	6.4	6.4	5.2
LC-BLYP	0.45	1.4	1.8	0.9	1.0	1.9	1.9	1.6
LC-PBE	0.75	−1.0	1.3	3.9	3.9	7.0	7.0	4.1
LC-PBE	0.55	3.1	3.1	1.7	1.9	4.3	4.3	3.1
LC-TPSS	0.75	−3.1	3.1	4.5	4.5	7.3	7.3	5.0
LC-TPSS	0.45	2.4	2.4	1.0	1.6	2.9	3.0	2.3
LC-M06-L	0.75	8.4	8.4	6.7	6.8	10.6	10.6	8.6
CAMY-B3LYP	0.34	−5.4	5.4	1.3	1.9	1.6	1.6	3.0
CAMY-B3LYP	0.20	−4.5	4.5	0.4	1.5	0.3	0.7	2.4

[a]All energies are in kilocalories per mole, and γ is in $1/a_0$. [b]Mean signed deviation. [c]Mean absolute deviation.

Table 2. Analysis of Calculated Reaction Energies of $PdCl^-$ as Compared to CCSD(T) Results[a]

		binding		$\Delta E^\dagger$		ΔE		total
	γ	MSD[b]	MAD[c]	MSD[b]	MAD[c]	MSD[b]	MAD[c]	MAD[c]
BP		−2.9	2.9	−2.2	2.2	−1.1	2.2	2.5
BLYP		−8.2	8.2	−1.2	1.5	−1.2	2.3	4.0
PBE		−1.5	1.6	−2.0	2.0	−0.6	1.9	1.9
TPSS		−3.5	3.5	−1.0	2.3	−1.3	2.6	2.8
M06-L		−3.5	3.5	2.2	2.7	2.4	2.6	2.9
B3LYP		−8.9	8.9	1.1	1.6	0.4	1.2	3.9
PBE0		−4.3	4.3	0.9	1.0	1.2	1.3	2.2
TPSSh		−4.6	4.6	−0.0	1.7	−0.7	2.1	2.8
M06		−5.7	5.7	4.3	4.5	6.4	6.4	5.5
LC-BP	0.75	0.8	1.2	2.5	2.5	2.4	2.4	2.0
LC-BP	0.60	2.9	2.9	1.1	1.2	1.8	2.0	2.0
LC-BLYP	0.75	−4.2	4.2	3.6	3.6	2.1	2.2	3.3
LC-BLYP	0.45	1.2	2.7	0.8	1.0	0.9	1.3	1.7
LC-PBE	0.75	−0.8	1.6	2.5	2.5	2.2	2.3	2.1
LC-PBE	0.55	2.1	2.1	0.6	1.3	1.4	1.9	1.8
LC-TPSS	0.75	−2.6	2.6	3.2	3.2	2.2	2.3	2.7
LC-TPSS	0.45	1.4	1.6	0.7	1.5	1.0	1.8	1.6
LC-M06-L	0.75	9.2	9.2	6.5	6.5	7.8	7.8	7.8
CAMY-B3LYP	0.34	−6.6	6.6	1.8	1.8	1.0	1.3	3.2
CAMY-B3LYP	0.20	−6.3	6.3	1.3	1.5	0.8	1.2	3.0

[a]All energies are in kilocalories per mole, and γ is in $1/a_0$. [b]Mean signed deviation. [c]Mean absolute deviation.

Table 3. Analysis of Calculated Reaction Energies of $PdCl_2$ as Compared to CCSD(T) Results

		binding		$\Delta E^\dagger$		ΔE		total
	γ	MSD[b]	MAD[c]	MSD[b]	MAD[c]	MSD[b]	MAD[c]	MAD[c]
BP		−3.7	3.9	−3.3	4.0	−5.1	5.3	4.4
BLYP		−9.1	9.1	−1.9	2.8	−5.0	5.0	5.7
PBE		−2.2	2.7	−3.3	3.8	−4.5	4.8	3.8
TPSS		−4.3	4.3	−1.7	2.9	−3.5	3.7	3.6
M06-L		−2.3	2.3	1.7	3.4	1.3	3.2	3.0
B3LYP		−8.2	8.2	1.4	1.6	0.3	1.1	3.6
PBE0		−3.0	3.3	1.0	1.4	2.2	2.2	2.3
TPSSh		−4.6	4.6	−0.2	2.5	−0.9	2.1	3.0
M06		−2.9	2.9	3.5	5.2	5.7	5.8	4.7
LC-BP	0.75	5.2	5.8	3.3	4.7	8.5	8.5	6.3
LC-BP	0.60	6.1	6.1	1.4	2.4	5.3	5.3	4.6
LC-BLYP	0.75	0.1	4.2	4.9	6.2	8.8	8.8	6.4
LC-BLYP	0.45	1.7	2.6	0.9	1.5	2.2	2.3	2.1
LC-PBE	0.75	3.5	4.8	3.5	5.0	9.0	9.0	6.2
LC-PBE	0.55	4.8	4.8	0.9	1.8	4.7	4.7	3.8
LC-TPSS	0.75	1.9	4.1	4.5	6.3	9.8	9.8	6.7
LC-TPSS	0.45	3.4	3.6	0.8	2.1	3.4	3.4	3.0
LC-M06-L	0.75	15.3	15.3	6.0	9.0	12.1	12.1	12.2
CAMY-B3LYP	0.34	−4.9	4.9	2.3	2.6	2.6	2.6	3.4
CAMY-B3LYP	0.20	−5.1	5.1	1.5	1.7	1.2	1.4	2.7

[a]All energies are in kilocalories per mole, and γ is in $1/a_0$. [b]Mean signed deviation. [c]Mean absolute deviation.

reaction energies with different functionals. The most relevant conclusion for the present study was that it was found that the best performing functionals were (meta) hybrids with a small admixture of exact exchange followed by local (meta)-GGAs with the (meta)-hybrids that include larger percentages of exact exchange performing the worst.

In their study Steinmetz and Grimme considered four energies for each system, the binding of the small molecule to the metal, the reaction barrier for the forward reaction, the barrier of the reverse reaction, and the energy of reaction from the complex to the products. We will not consider the reverse reaction here to keep the analysis consistent with how we treat the Grubbs catalyst. Thus, we include the following three energies in our analysis of the small-molecule reactions: the metal-molecule binding energy, the complex to transition state energy (the kinetic barrier), and the complex to product energy (the thermodynamic barrier). Neglecting the fourth energy, the barrier of the reverse reaction changes the quantitative results somewhat but does not change the qualitative conclusions. The 41 reactions and 3 energies per reaction give a total of 123 data points.

Table 4. Analysis of Calculated Reaction Energies of a Ni Atom As Compared to CCSD(T) Results[a]

		binding		$\Delta E^{\dagger}$		ΔE		total
	γ	MSD[b]	MAD[c]	MSD[b]	MAD[c]	MSD[b]	MAD[c]	MAD[c]
BP		8.7	8.7	−2.8	2.8	−1.6	2.0	4.5
BLYP		1.2	2.1	−3.1	3.1	−4.0	4.0	3.0
PBE		8.9	8.9	−1.8	2.8	0.0	2.5	4.7
TPSS		7.5	7.5	−1.6	2.5	−1.8	3.1	4.4
M06-L		12.5	12.5	−0.1	2.2	−1.0	2.4	5.7
B3LYP		−5.0	5.0	−0.8	2.3	−2.4	2.5	3.3
PBE0		1.5	3.0	−0.2	1.6	0.3	1.5	2.1
TPSSh		5.4	5.4	−1.3	1.9	−2.1	2.2	3.2
M06		−0.8	2.6	1.5	2.3	4.3	4.3	3.0
LC-BP	0.75	3.0	3.6	2.4	3.4	6.2	6.3	4.4
LC-BP	0.60	7.4	7.4	1.5	2.8	5.8	6.1	5.4
LC-BLYP	0.75	−4.5	4.5	2.3	2.8	3.8	3.9	3.7
LC-BLYP	0.45	4.5	4.5	0.2	1.7	2.6	3.1	3.1
LC-PBE	0.75	1.5	2.7	2.1	3.1	5.7	6.0	3.9
LC-PBE	0.55	7.6	7.7	1.2	2.7	5.8	6.2	5.5
LC-TPSS	0.75	1.0	2.9	2.2	3.2	4.5	5.0	3.7
LC-TPSS	0.45	9.1	9.1	0.8	2.4	4.0	4.9	5.4
LC-M06-L	0.75	13.9	13.9	3.9	4.4	6.0	6.1	8.1
CAMY-B3LYP	0.34	−3.9	3.9	0.1	2.0	−0.7	2.1	2.7
CAMY-B3LYP	0.20	−2.6	2.8	−0.4	2.1	−1.3	2.3	2.4

[a]All energies are in kilocalories per mole, and γ is in $1/a_0$. [b]Mean signed deviation. [c]Mean absolute deviation.

Table 5. Analysis of Calculated Reaction Energies of All Small Systems As Compared to CCSD(T) Results

		binding		$\Delta E^{\dagger}$		ΔE		total
	γ	MSD[b]	MAD[c]	MSD[b]	MAD[c]	MSD[b]	MAD[c]	MAD[c]
BP		1.1	4.2	−3.3	3.5	−3.4	3.8	3.8
BLYP		−4.9	5.6	−2.7	3.0	−4.0	4.3	4.3
PBE		2.1	3.9	−3.0	3.3	−2.5	3.5	3.6
TPSS		−0.3	4.1	−2.1	3.0	−2.9	3.6	3.5
M06-L		0.8	4.5	1.0	2.8	0.8	2.6	3.3
B3LYP		−7.2	7.2	0.3	1.8	−0.6	1.4	3.5
PBE0		−2.3	3.3	0.5	1.2	1.3	1.6	2.0
TPSSh		−1.8	4.2	−0.9	2.2	−1.5	2.3	2.9
M06		−4.0	4.4	3.2	3.9	5.7	5.7	4.7
LC-BP	0.75	2.3	2.8	3.1	3.6	5.9	6.0	4.1
LC-BP	0.60	4.8	4.8	1.6	2.1	4.4	4.5	3.8
LC-BLYP	0.75	−3.4	4.3	3.9	4.3	5.3	5.3	4.7
LC-BLYP	0.45	2.1	2.8	0.7	1.3	1.9	2.1	2.0
LC-PBE	0.75	0.6	2.4	3.1	3.6	6.0	6.1	4.0
LC-PBE	0.55	4.2	4.2	1.1	1.9	4.0	4.2	3.5
LC-TPSS	0.75	−1.0	3.1	3.7	4.3	6.0	6.1	4.5
LC-TPSS	0.45	3.9	3.9	0.8	1.9	2.8	3.2	3.0
LC-M06-L	0.75	11.3	11.3	5.9	6.7	9.2	9.2	9.1
CAMY-B3LYP	0.34	−5.2	5.2	1.4	2.1	1.2	1.9	3.1
CAMY-B3LYP	0.20	−4.6	4.7	0.7	1.7	0.3	1.3	2.6

[a]All energies are in kilocalories per mole, and γ is in $1/a_0$. [b]Mean signed deviation. [c]Mean absolute deviation.

The mean absolute deviations (MADs) and mean signed deviations (MSDs) are summarized in Tables 1−5. Tables 1−4 summarize the Pd, $PdCl^-$, $PdCl_2$, and Ni results, respectively. The averages across all metal systems are presented in Table 5. Averages for the binding energy of the molecule to the metal, the kinetic barrier to the reaction ($\Delta E^{\dagger}$) and thermodynamic barrier (ΔE), and across all reaction types (total) are included. In most cases both MADs and MSDs are included. The signed errors were defined as the result calculated with the given functional minus the CCSD(T) result so that a negative signed error indicated a result smaller or more negative than the CCSD(T) value and a positive signed error indicated a larger or more positive result than the benchmark value.

The individual reaction energies that are averaged to the MADs and MSDs can be found in the Supporting Information.

Since the main point of interest is the performance of the range-separated functionals in comparison with the standard functionals, we will frame the discussion in terms of the different classes of functional (local, global hybrid, and range-separated).

Starting with the local functionals (BP, BLYP, PBE, TPSS, and M06-L), we see that the overall errors (total from Table 5)

dx.doi.org/10.1021/ct301112m | J. Chem. Theory Comput. 2013, 9, 2286−2299

are in the range 3.3−4.3 kcal/mol with M06-L being about the best performed local functional and BLYP about 0.5 kcal/mol worse than the next worst functional. Similar trends are observed for all of the Pd systems (Tables 1−3) though the average errors for these systems were typically a little lower, especially for reactions involving the Pd atom and $PdCl^-$. For the Ni reactions, the trend with respect to functional is reversed with BLYP having the lowest average error and M06-L the highest.

In terms of the different reaction steps, the most problematic step for the local functionals was the initial binding of the metal atom/molecule to the small molecule. The MAD across all systems was highest for this step for all functionals. For the Pd systems, the binding was typically too small and BLYP typically performed the worst while for the Ni systems the binding was much too large on average and BLYP had the lowest average error and M06-L the highest. The local functionals with few to no empirical parameters (BP, BLYP, PBE, TPSS) underestimated the kinetic barriers in all cases and gave overall errors in the range of 3.0 (TPSS and BLYP) to 3.5 (BP) kcal/mol for this step. The more highly parametrized M06-L was significantly better for this step, showing no particular tendency to overestimate or underestimate the barrier and having the smallest overall average error of the local functionals of 2.8 kcal/mol. The results for the thermodynamic barrier are similar to those of the kinetic barrier. The signed errors are negative across the board for the less parametrized functionals and are overall close to zero for M06-L. M06-L is the best local functional for this property with an MAD of 2.6 kcal/mol.

Turning now to the global hybrids, we see that in general adding global exact exchange improves the results a little. The overall total average errors now range from 2.0 (PBE0) to 4.7 (M06) kcal/mol. In most cases the global hybrids performs better than the corresponding local functionals for each of the four types of metal complex under consideration. The exception is M06 which overall performs worse than M06-L and is worse than M06-L for all of the Pd systems but is significantly better for the Ni reactions. The addition of exact exchange typically weakens the complexation energy and increases the kinetic and thermodynamic barriers. This leads to worse binding energies for the Pd systems and improved binding energies of the Ni systems. The kinetic and thermodynamic barriers for both Pd and Ni are typically improved. Again, the Minnesota functionals are an exception here where M06 is typically not an improvement over M06-L except for the binding energies of the small molecules to Ni.

The results for the standard functionals agree quantitatively with those reported by Steinmetz and Grimme,[40] as would be expected. The trend of decreasing accuracy with increasing exact exchange noted earlier is not reflected in the present results because of the lack of high exact exchange functionals such as BHandH or M06-2X in the present set of functionals. The only differences between the present results and those from the Steinmetz and Grimme paper are found in the Ni-small molecule binding energies evaluated with the M06-L functional. In the current study the binding energies are in rather worse agreement with the reference data than those reported previously.[40] This is due to the differing treatments of the Ni atom. The ADF program is able to use symmetry to prevent orbitals of differing l from mixing whereas the codes used in the previous study were unable to prevent some mixing leading to different energies for the Ni atom evaluated with M06-L.

For most of the range-separated functionals, two sets of results are reported. In the first, the recommended values of the γ parameter are used. A γ of 0.75 $1/a_0$ for LC-type and 0.34 $1/a_0$ for CAMY-B3LYP has been suggested.[19] The second set of results utilize a value of γ that is optimized in order to minimize the MAD across all 41 reactions for that functional. In all cases a smaller value of γ was found to improve the overall MAD.

A comment about LC-M06-L should be made at this point. In all cases, the range-separated form of M06-L performed much worse than the standard M06-L functional. A few attempts at optimizing γ found that the optimal value is close to zero which corresponds to no exact exchange. This result is not especially surprising as M06-L has a large number of parameters that have been optimized against experimental data. Adding anything new to the functional is likely to destroy the optimal nature of the functional unless all of the parameters are adjusted to allow for the change. Truhlar and co-workers have created highly parametrized functionals that include range-separation as part of the form of the functional in their M11 set of functionals.[21,75] These functionals utilize an error function as the switching function in eq 1. We do not have the capability of creating an optimized form of M06-L or M11 that includes range-separation through a Yukawa potential and will therefore not place much emphasis on the LC-M06-L functional from here on.

In considering the rest of the range-separated functionals we shall compare them with their parent functional. BP, BLYP, PBE, and TPSS are the parent functionals of LC-BP, LC-BLYP, LC-PBE, and LC-TPSS, respectively, and we take B3LYP as the parent of CAMY-B3LYP.

In the case of the range separated functionals with standard values of γ, for the most part they provide results that represent a small improvement upon their parent. The exception is LC-TPSS that has an overall MAD slightly bigger than that of TPSS. The introduction of range-separation significantly improves the results of the Ni calculations but improves only some of the Pd results. As was the case with the global hybrids, the addition of range separation increases both the kinetic and thermodynamic barriers. The effect is greater than that seen for the global hybrids and the range-separated barriers are on average too high by about the same amount as the barriers calculated with the local functionals are too low. The effect of range-separation on the metal−small molecule binding is different from that of the introduction of global exact exchange. When global exchange is introduced, the binding energies are reduced on average, but when range-separation is introduced, binding energies are increased on average.

As has already been noted, the optimized values of γ are all less than the suggested value. Smaller values of γ correspond to a greater contribution of the DFT exchange and a decreased contribution from the exact exchange. As would be expected, this leads to a lowering of the kinetic and thermodynamic barriers which are then significantly improved with the optimized values of γ. In contrast, decreasing γ seems to increase the influence of exact exchange on binding energies leading to even larger increases in the metal−small molecule binding energies as compared to the corresponding local DFT values. This somewhat counterintuitive result will be considered further in later sections.

Overall, we find that the addition of range-separated exchange to a functional gives a small improvement over the parent functional, particularly if an optimized value of γ is used. However, the range-separated functionals do not represent a

Table 6. Analysis of Calculated Energies of Model Grubbs Reaction As Compared to CCSD(T) Results[a]

	γ	1 → 2	2 → 3-cis	2 → 3-tr	3-cis → TS-cis	3-tr → TS-tr	TS-cis → 4-cis	TS-tr → 4-tr	MSD[b]	MAD[c]
best estimate[b]		25.2	−7.7	−17.6	0.5	8.8	−13.2	−10.4		
BP		17.5	−1.0	−9.5	1.4	9.1	−12.0	−10.6	1.3	3.6
BLYP		13.2	6.2	−4.3	2.0	10.3	−7.9	−7.0	3.8	7.3
PBE		19.2	−3.5	−11.5	1.4	8.9	−13.3	−11.7	0.6	2.7
TPSS		19.7	−3.2	−11.8	1.1	8.0	−11.2	−9.0	1.2	3.0
M06-L		18.7	−2.7	−13.5	0.7	8.5	−14.7	−11.6	0.0	2.7
B3LYP		15.2	5.8	−5.9	0.4	7.3	−10.6	−8.5	2.6	5.9
PBE0		20.0	−1.7	−11.5	0.6	5.4	−15.8	−12.8	−0.4	3.8
TPSSh		19.7	−2.4	−11.5	0.5	6.5	−12.3	−9.6	0.8	3.0
M06		22.0	−4.0	−15.3	−0.2	6.4	−14.0	−10.9	−0.2	1.9
LC-BP	0.75	28.1	−9.2	−20.2	−2.7	2.7	−21.4	−16.2	−3.5	4.3
LC-BP	0.90	27.8	−7.6	−19.4	−3.4	1.9	−22.1	−16.2	−3.5	4.3
LC-BLYP	0.75	24.0	−2.0	−15.2	−2.2	3.9	−17.3	−12.7	−1.0	3.3
LC-BLYP	0.20	24.3	−8.4	−17.8	1.1	7.9	−12.7	−10.2	−0.2	0.5
LC-PBE	0.75	26.6	−7.5	−18.2	−2.8	2.5	−22.2	−17.0	−3.4	3.9
LC-PBE	0.70	26.7	−8.1	−18.5	−2.5	2.8	−22.0	−16.9	−3.4	3.9
LC-TPSS	0.75	26.0	−6.2	−17.5	−2.9	2.4	−20.8	−15.5	−2.9	3.6
LC-TPSS	0.60	26.6	−8.2	−18.5	−2.1	3.2	−20.0	−15.1	−2.8	3.2
LC-M06-L	0.75	39.3	−25.4	−38.5	−2.7	3.5	−20.8	−13.8	−6.3	10.3
CAMY-B3LYP	0.34	19.0	2.1	−10.2	−0.4	6.3	−12.5	−9.5	1.3	4.0
CAMY-B3LYP	0.25	18.9	1.8	−10.3	−0.1	6.7	−12.1	−9.3	1.5	4.0

[a]All energies are in kilocalories per mole, and γ is in $1/a_0$. [b]Mean signed deviation. [c]Mean absolute deviation.

clear improvement over standard global hybrids or the M06-L functional.

3.2. Grubbs Catalyst. *3.2.1. Model Grubbs Catalyst.* The metathesis reaction performed by the model catalyst $[(PH_3)(NHC)Cl_2Ru{=}CH_2]$ is depicted in Figure 2. We will make use of the notation suggested by Zhao and Truhlar to label the reaction stationary points.[73] We depart from the earlier study in the definitions of the energies of interest. As was noted in section 2.3, the choice of zero energy point in a reaction profile can affect the calculated average errors. Zhao and Truhlar chose the activated catalyst (**2**) as the zero point. This choice puts great emphasis on the ability of a calculational method to predict the metal−alkene binding energy. In order to try and weight all steps in the reaction equally, rather than evaluating energies relative to an arbitrarily chosen zero point, we consider energy differences between neighboring species in the reaction profile. Thus our energies of interest include the energy difference between species **1** and **2**, **2** and **3-cis**, **2** and **3-trans**, **3-cis** and **TS-cis**, and so on.

The calculated energy differences are presented in Table 6. Considering first the standard functionals, M06 (MAD 1.9 kcal/mol) and M06-L (2.7 kcal/mol) perform well and the functionals including the LYP correlation functional BLYP (7.3 kcal/mol) and B3LYP (5.9 kcal/mol) perform least well. This is similar to what was observed[73] earlier but with a considerably smaller range of MADs. The non-LYP standard functionals perform almost as well as M06-L with average errors in the range 2.7−3.8 kcal/mol. All of the functionals do a good job of describing the reaction of the **3** → **4** isomerization but less well at describing the phosphine dissociation **1** → **2** and ethene association **2** → **3**. These energies are all underestimated by the standard functionals with M06 showing the smallest underestimations.

Similarly to the small-molecule reactions, Table 6 includes results with the suggested values of γ for each range-separated functional and with values of γ that minimize the MAD. In general, the addition of range-separation does not improve the results and the optimization of γ leads to little improvement. The exception are the LYP-based functionals and LC-M06-L. LC-BLYP with γ of 0.75 $1/a$ is a significant improvement over BLYP and the rather small γ value of 0.20 $1/a$ gives extremely good results with LC-BLYP. CAMY-B3LYP represents an improvement over B3LYP but optimization of γ does not change the MAD significantly. LC-M06-L is much poorer than M06-L. For all functionals the addition of range-separation increases all of the catalyst−phosphine ligand and catalyst−ethene interactions leading to improved agreement with the best estimates. The transition states are lowered relative to the catalyst−ethene complexes, and the products are lowered in energy relative to the transition states leading to a worsening relative to the best estimates.

Overall, the introduction of range separation does not lead to an improvement except for the LYP-based functionals that were relatively poor to start with.

3.2.2. Real Grubbs Catalyst. The loss of a phosphorus ligand has been shown to be an important and rate-determining step in the operation of real Grubbs catalysts. Many older functionals have performed poorly in describing this reaction.[42,44,73] The Minnesota functionals have performed better[73] as have older functionals with dispersion corrections added.[42,44] It thus seems that the incorrect treatment of dispersion (and perhaps medium-range correlation[76−79]) is responsible for the large errors found when calculating phosphine ligand−catalyst interactions in realistic models of the Grubbs catalyst.

We would therefore expect that range-separated functionals would not be an improvement upon their parent functionals. Range-separated functionals explicitly designed to describe weak interactions correctly have been created,[24,80−82] but typical RS-functionals would not be expected to include dispersion. In going from BP to LC-BP, a portion of the DFT exchange is replaced with Hartree−Fock exchange. The Hartree−Fock level of theory does not include dispersion and exact exchange would not be expected to provide a major

improvement. The correlation contribution is only modified indirectly through the density change caused by the modification of the exchange part of the functional, and there should be no mechanism for improving the description of medium-range correlation.

The results of our study (Table 7) were therefore somewhat surprising to us. The calculated binding energies of $P(Cy)_3$ to the real catalyst with standard functionals follow the same trends as observed previously.[73] The binding energies are all strongly underestimated with the exception of those predicted by the M06 and M06-L functionals. The binding energies calculated with all of the LC functionals except LC-M06-L are a major improvement over the local functional results. The improved functionals all give binding energies within 7 kcal/mol of the experimental value with LC-BP being the best with an error of 3.0 kcal/mol. The CAMY-B3LYP functional improves upon B3LYP but still predicts a binding energy that is too low by about 20 kcal/mol.

Table 7. Phosphine Binding Energies of Real Grubbs II Catalyst[a]

	γ	
expt		40.2
BP		12.6
BLYP		3.1
PBE		18.9
TPSS		15.7
M06-L		41.8
B3LYP		8.1
PBE0		20.5
TPSSh		15.1
M06		38.7
LC-BP	0.75	43.2
LC-BLYP	0.75	33.8
LC-PBE	0.75	36.8
LC-TPSS	0.75	35.8
LC-M06-L	0.75	118.8
CAMY-B3LYP	0.34	19.5

[a]All energies are in kilocalories per mole, and γ is in $1/a_0$.

It would appear that RS-functionals are doing a good job of describing the Ru to $P(Cy)_3$ binding of the real Grubbs catalyst.

This surprising result along with the unusual dependence of the metal−small molecule binding energies on the attenuation parameter γ (section 3.1) prompted us to examine more closely exactly what is going on when a local functional is converted into its range-separated form. The results of these investigations are reported in the next sections.

3.3. Analysis of Interactions in Range-Separated Calculations. *3.3.1. Water Dimer.* The size of the real Grubbs catalyst makes it an impractical target for detailed analysis studies. We therefore chose a much simpler system for our initial study: the water dimer. $(H_2O)_2$ obviously does not include a transition metal, but it is an extremely simple system amenable to detailed studies. The bond between the two H_2O molecules also includes a significant dispersion contribution. A large portion of the error in the predicted ligand−Ru binding energy in the real Grubbs catalyst can be attributed to the neglect of dispersion.[42−44] From the results in the previous section, it seems that the LC functionals introduce something that mimics dispersion. We therefore thought that it would be of interest to see how the LC functionals perform when describing another bond that includes dispersion.

The binding energy of the water dimer at the geometry specified by Grimme and co-workers[76] for all of our functionals of interest can be found in Table 8 along with a benchmark CCSD(T) value for comparison. Also included is the "HF-LYP" functional. This is the functional consisting of 100% exact exchange, no DFT exchange and the LYP correlation functional. This functional is included to provide the limiting value of the LC-BLYP functional as $\gamma \rightarrow \infty$. The standard BLYP functional is the limit as $\gamma \rightarrow 0$.

Table 8. Binding Energies of the Water Dimer[a]

	γ	
CCSD(T)[b]		5.02
BP		4.06
BLYP		4.01
PBE		4.89
TPSS		4.36
M06-L		4.48
B3LYP		4.39
PBE0		4.85
TPSSh		4.36
M06		4.50
HF-LYP		5.96
LC-BP	0.75	6.26
LC-BLYP	0.75	6.26
LC-PBE	0.75	5.57
LC-TPSS	0.75	5.38
LC-M06-L	0.75	9.24
CAMY-B3LYP	0.34	5.24

[a]All energies are in kilocalies per mole, and γ is in $1/a_0$. [b]The complete basis set extrapolated value is from ref 74.

As would be expected since they neglect dispersion, the local and global hybrid functionals underestimate the binding energy of the water dimer relative to the CCSD(T) value. The range-separated functionals all predict binding energies greater than the benchmark value. Thus we again find that converting a local or global hybrid functional to a range-separated functional results in an interaction energy between two closed shell molecules that is greater than that obtained from the parent functional. The HF-LYP interaction energy is 5.96 kcal/mol and greater than the BLYP value (4.01 kcal/mol) and the benchmark value (5.02 kcal/mol). The LC-BLYP value is greater still at 6.26 kcal/mol. Naively, we would have expected it to be intermediate between the BLYP and HF-LYP results.

To investigate this result further, we have evaluated the binding energy of the water dimer with the LC-BLYP functional for a range of values of the range-separation attenuation parameter γ and analyzed these energies using the bonding analysis developed by Morokuma[83] and Ziegler and Rauk.[84] In this analysis, the interaction of two subsystems (or fragments) is divided into four pieces.

$$\Delta E = \Delta E_{\text{prep}} + \Delta E_{\text{elst}} + \Delta E_{\text{Pauli}} + \Delta E_{\text{oi}} \quad (2)$$

The interaction energy ΔE is defined as the difference in energy between the two isolated fragments and the final system where the two fragments are bound together. The first part of the analysis is the preparation energy ΔE_{prep} which is the energy required to distort the fragments from the geometries they show when isolated to the their geometries in the geometry of

interest. In our case, the geometry of the two separated water molecules are chosen to be the same as their geometries in the complex and ΔE_{prep} is therefore zero. The second term, the electrostatic term ΔE_{elst} is the classical electrostatic interaction between the charge densities of the unperturbed fragments brought into the geometrical arrangement corresponding to the final structure. The third term, the Pauli energy ΔE_{Pauli}, is the energy cost of reorthogonalizing the occupied fragment orbitals once the two fragments have been brought close together. Finally, the orbital term ΔE_{oi} corresponds to the energy gained as the orbitals of the fragments are allowed to relax to form the self-consistent orbitals of the total system.

To simplify the analysis we will apply the range-separated functional in a post-SCF fashion. By this, we mean that orbitals and density were obtained through solution of the Kohn−Sham equations with the standard BLYP functional and the range separation was only introduced in the evaluation of the energy using the BLYP density. By taking this approach, all of the contributions to the energy that do not depend on the exchange functional or exact exchange are independent of γ and can be ignored for the present discussion. By definition, the electrostatic component of the interaction energy ΔE_{elst} is derived from the Coulomb and nucleus−electron interactions. In the water-dimer calculations, it will therefore be independent of γ. We shall thus limit ourselves to the XC and HF parts of the Pauli and orbital terms.

The important contributions and total interaction energy as a function of γ are plotted in Figure 4. Since the Pauli term (blue line) is the most important we divide it into LDA (black line), GGA (red line), and HF (green line) parts. The orbital term (yellow line) is less important, and we only present the total term. The total interaction (purple line) increases rapidly with γ from the BLYP value of 4.01 kcal/mol to a maximum of 6.8 kcal/mol at γ = 0.25 $1/a_0$ and then slowly decreases as γ increases. Test calculations found that the effects of not including range-separation self-consistently are relatively small. The binding energy at γ = 0.75 $1/a_0$ in Figure 4 where range-separation is included post-SCF is less that 0.1 kcal/mol smaller than the value from Table 8 where range-separation is included in the evaluation of the energy and the Kohn−Sham potential.

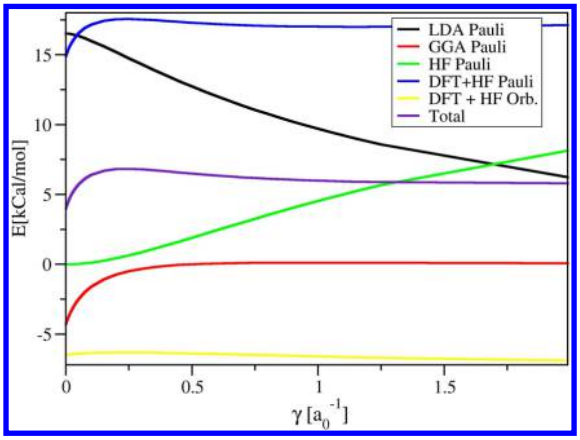

Figure 4. Bond analysis of interaction energy of water dimer as a function of range-separation parameter γ.

The increase in binding energy for small values of γ is clearly due to the GGA exchange part of the Pauli interaction. The GGA term (red line in Figure 4) is significantly destabilizing in the pure BLYP calculation and disappears rapidly with increasing γ. Of the other terms, the orbital contribution (yellow line) changes little over the range of γ considered but does contribute to the slow decrease of the interaction energy beyond γ = 0.25 $1/a_0$. The LDA (black line)and HF exchange (green line) vary gradually as γ increases and any changes in the LDA term are largely canceled by changes in the HF term.

How can we explain this behavior? The LDA approximation typically predicts bonds that are too strong. This is certainly true for the water dimer where the calculated binding energy is 7.7 kcal/mol with the VWN5 functional. Gradient corrections destabilize bonds improving the agreement with benchmark data. The regions of space where GGAs contribute the most to the total energy are those where $|\nabla\rho|/\rho$ is high, which most often are regions of low density. These low density regions are stabilized by GGAs. When two fragments form a bond a part of the low density region around each atom is converted into a bonding region. Some of the low-density stabilization is lost leading to an overall destabilization by the GGA of the molecule relative to the separated fragments.

If we now include range separation with a small value of γ, only very large values of r_{12} will be affected. Electrons are further apart in regions of low density.[85,86] Thus, for small values of γ in low density regions the electron exchange will be described by HF exchange and by DFT exchange in higher density regions. As discussed in the previous paragraph, these low density regions are where significant stabilization comes from the GGAs and lead to the destabilization of chemical bonds. At low values of γ, range separation essentially removes the influence of the GGA on chemical bonding and we are left with LDA that is more gradually mixed with exact exchange. By going to only LDA DFT exchange, we return to a regime of overbinding that is responsible for the too large interaction energies of the water dimer, the increased binding energies of the small molecules with the metal systems, and the significantly increased binding energies of the phosphine ligand to the Ru atom in the model and real Grubbs catalysts.

The introduction of range separation mimicking the dispersion interaction has been noticed previously.[38,87] In the first study, Scuseria and co-workers noted that the LDA-based model of the exchange hole employed by Hirao and co-workers to develop RS-functionals led to excessive delocalization for larger values of the reduced gradient and to overbinding for smaller values of γ.[87] Steinman and co-workers considered hydrocarbon reaction energies, and it was found that range-separated functionals perform better than local functionals or global hybrids.[38] The reaction energies calculated typically included significant contributions from dispersion.

3.3.2. Small Molecule−Metal Reactions. In the previous section a detailed analysis of the effect of introducing range-separation on the interaction of two water molecules was described. In this section we perform similar analyses of a few representative reactions from the Steinmetz−Grimme test set.

The first step in all of these reactions is the binding of the small molecule to the metal center. This is similar to the water dimer in that it involves bringing two closed shell molecules together from large separation to form a bound system. The analyses of the small molecule−metal binding reactions are all qualitatively similar to that of the water dimer. An analysis of the $P(Cy)_3$ ligand with the real Grubbs catalyst also produced qualitatively similar results. Given that nothing new was produced we will not discuss these reactions further. We shall rather focus on the kinetics and thermodynamic barriers in this section.

After analyzing a number of the reaction from the Steinmetz−Grimme data set in detail, it is clear that the results vary from reaction to reaction and unlike the small molecule to metal center binding, one analysis can not be used to represent all of the systems considered here. Some analyses are pictured in Figures 5−8. A few outcomes are observed consistently, and we will discuss them in the next few paragraphs.

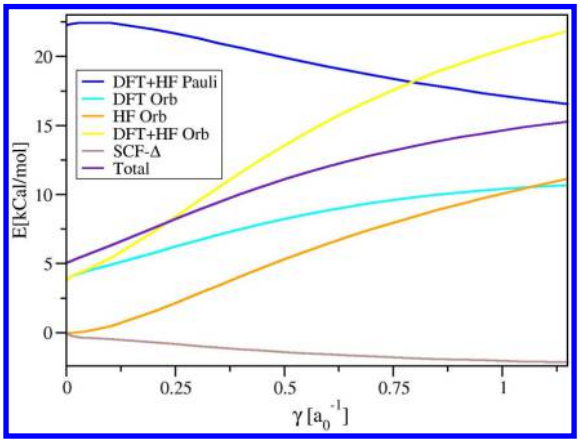

Figure 5. Bond analysis of kinetic barrier of reaction of BH_3 with an Ni atom as a function of range-separation parameter γ.

We should first note the obvious difference between the metal−molecule binding energies and the kinetic and thermodynamic barriers. The first measures the energy difference between two separate molecules and a complex while the latter two energies correspond to the difference in energy between two structural isomers. As a consequence, a bonding analysis in terms of bringing two fragments together is not possible. Instead, we can consider the two structures of interest (e.g., the metal−small molecule complex and the transition state in the case of the kinetic barrier) as two systems formed from a number of atomic fragments. The binding energy of the two systems will be formed from electrostatic, Pauli, and orbital terms as before. The kinetic barrier can thus be described in terms of how these terms change between the two structures of interest. Of most interest for our purposes is how the contributions to the kinetic and thermodynamic barriers change as γ is changed.

Analyses of two example reactions are presented in in Figures 5−8. It would be expected that as rearrangements rather than association reactions these reactions would be less sensitive to the Pauli interaction and more sensitive to the orbital relaxation. This is reflected in the analyses. The change in the Pauli term is not always non-negligible, but in no example does it dominate. In a few cases it makes a significant contribution to the trend of the total energy difference. Since the Pauli term is less important in this case, we only present the total Pauli term (dark blue line in Figures 5−8) and do not consider the individual contributions from the functional and exact exchange. We do separate the orbital term (yellow line) into contributions from the functional (light blue line) and from exact exchange (orange line). We have also included the influence of range-separation in the potential used to calculate the orbitals causing the density to become dependent on γ. The energy terms not dependent on the functional or exact exchange become indirectly dependent on γ through the self-consistent field procedure. We lump all of these terms together as "SCF terms". The sum of all nonfunctional and nonexact exchange dependent terms can be quite large. We are only interested in how the energy changes as γ is varied, and we therefore consider the change in the SCF terms as γ varies from zero, a contribution we shall call SCF-Δ (brown line).

The kinetic barriers are almost all strongly influenced by the HF orbital contribution. As γ increases, this term becomes more positive and the overall barrier heights become more positive. The contribution of the DFT part of the orbital term is less consistent. It is always positive for $\gamma = 0$ but examples were found where it increases, decreases, or is largely unchanged as γ increases. The Pauli and SCF-Δ terms generally decrease as γ increases.

If increasing γ can be thought of as "turning on" exact exchange in some sense then what is observed is consistent with what is seen with global hybrids. Increasing exact exchange leads to higher reaction barriers.[88]

In contrast to the small-molecule binding, the kinetic barrier and the contributions to it from the bonding analysis do not change smoothly with γ. The behavior for smaller values of γ is not always the same as for larger values of γ indicating that the short and long-range contributions are not equally important. For example, in Figure 7 the DFT Orbital term for the kinetic

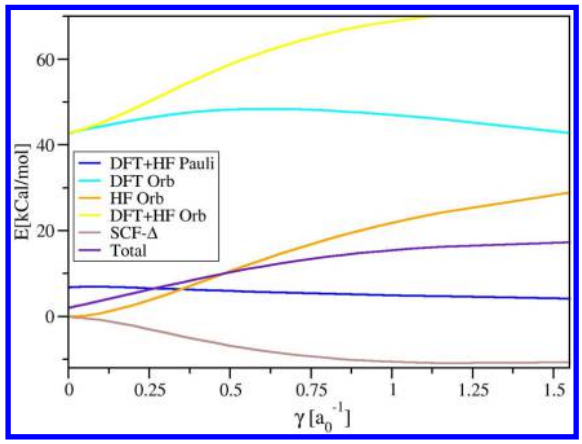

Figure 6. Bond analysis of thermodynamic barrier of reaction of BH_3 with a Ni atom as a function of range-separation parameter γ.

barrier of the Pd−H_2 reaction changes little over the range of values of γ typically employed in calculations (the long-range interaction is removed). At the same time, the exact exchange

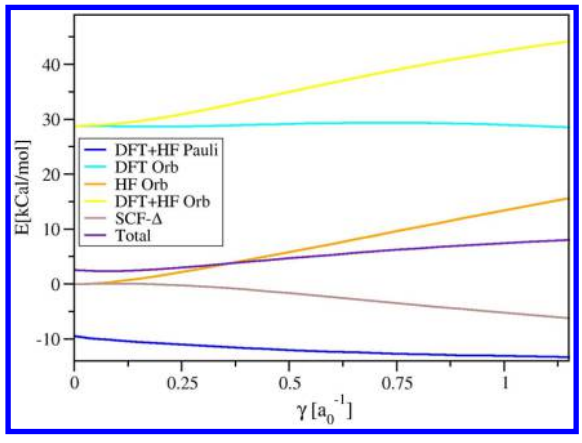

Figure 7. Bond analysis of kinetic barrier of reaction of H_2 with a Pd atom as a function of range-separation parameter γ.

orbital term increases steadily as the long-range interaction is introduced. As γ increases further the DFT orbital term decreases dramatically as the mid- to short-range interaction is removed while the HF orbital term continues to increase as the mid and short-range interaction is introduced. Thus for this reaction the DFT contribution is dominated by the short-range interactions that are not modified significantly when γ is small while the exact exchange contribution is influenced by both the long and short-range regions. In contrast, we see that for the reaction of Ni with BH_3 (Figure 5), both the HF and DFT orbital contributions to the kinetic barrier become more positive from $\gamma = 0-1.25$ but as γ increases to a very large value the DFT orbital term becomes small and the HF orbital terms increases only slightly. We see therefore for this reaction that for the DFT term the long and short-range interactions are important and lead to contributions of opposite sign while for the exact exchange term the long-range part of the interaction is more important.

Much of the qualitative discussion concerning the kinetic barrier also applies to the thermodynamic barrier. The trend observed as a function of γ is again determined largely by the orbital term and in particular the exact exchange part of the orbital term. Most often the thermodynamic barrier increases with increasing γ. A few examples were found where the Pauli, SCF, and DFT orbital terms are relatively important and where the total energy does not increase monotonically with γ.

The difference in long-range and short-range behavior also appears in the thermodynamic barriers. We consider again the examples of the reaction of H_2 with Pd (Figure 8) and BH_3 with Ni (Figure 6). In the case of H_2 with Pd, the behavior for the thermodynamic barrier is similar to that of the kinetic barrier. The DFT orbital term changes little for small values of γ (the long-range interaction is removed) but then decreases significantly as γ increases further (the short-range interaction is removed). The HF orbital term increases consistently as first the long-range interaction is added and then the short-range interaction is added. The trends of the thermodynamic barrier of the reaction of BH_3 with Ni are similar to those of H_2 with Pd. The DFT orbital term changes little as γ goes from 0 to 1.5 $1/a_0$ but decreases significantly thereafter and the exact exchange term increases steadily as γ increases.

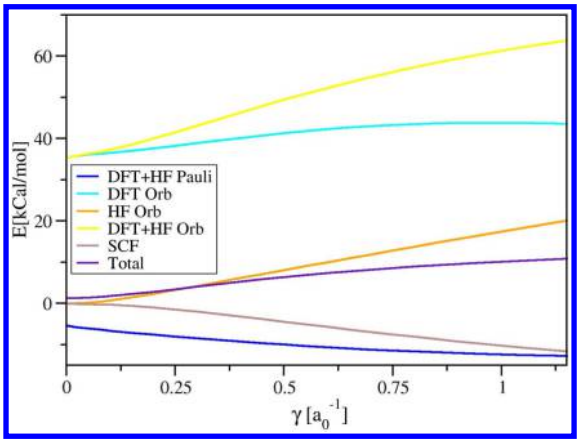

Figure 8. Bond analysis of thermodynamic barrier of the reaction of H_2 with a Pd atom as a function of range-separation parameter γ.

4. CONCLUSIONS

In this paper we examined the performance of range-separated functionals in the prediction of reaction profiles involving transition metals using high-level wave function results as benchmark data.

The performance of RS-functionals was somewhat superior to that of few to no parameter local GGAs or meta-GGAs for a set of 41 reactions involving Ni and Pd systems but was not significantly superior to that of global hybrids or the highly parametrized local functional M06-L. Optimization of the attenuation parameter γ improved the performance somewhat but the optimal value of γ seems to depend on the identity of the metal atom involved. The overall optimized value was biased toward Pd because the data set included a majority of Pd systems and optimizing γ actually worsened the quality of the results for the reactions involving Ni.

The second benchmark data set consisted of results describing a model Grubbs catalyst. The introduction of range-separation only improved the BLYP and B3LYP functionals that had initially provided the worst results from the set of standard functionals. Somewhat surprisingly, the inclusion of range-separation significantly improved the prediction of Ru−$P(Cy)_3$ interaction energies of real Grubbs catalysts. This results was unexpected as previously observed errors in calculation of this energy were attributed to neglect of dispersion and incorrect medium-range correlation. Neither of these problems should be solved through range-separation.

These somewhat curious results led us to analyze in more detail first the water dimer, a simple bond that is significantly influenced by dispersion as well as the metal−small molecule binding and the Ru−$P(Cy)_3$ interaction of the real Grubbs catalyst. All of these interaction energies are increased by the introduction of range-separation. A bonding analysis revealed that range-separation was selectively turning off the gradient-dependent part of the functional leading to LDA-type overbinding results. It thus seems that range-separation can be used to fix errors caused by the absence of dispersion corrections in standard functionals but that the improvements observed are due to cancellation of error rather than any improvement in the functional. We would therefore suggest caution in the use of RS-functionals in studies where dispersion is critical as it is not yet known how consistent the error-cancellation will be. The work of Scuseria and co-workers found that this overbinding was due to the ansatz of the exchange hole used to create the RS-functionals.[87] RS-functionals based upon hole models more appropriate for GGAs should not show this overbinding behavior.

Similar analyses of the kinetic and thermodynamic barriers of model reactions found more expected behavior. The interaction between the influence of the functional and exact exchange as range-separation was turned on was complicated and system dependent. A few general trends were observed and in particular it was found that long-range exact exchange was the most influential contribution and led to higher barriers.

In summary, we do not find RS-functionals to be decisively superior to conventional functionals across the range of systems we have considered. In fact, we find that closed shell-closed shell interactions are artificially stabilized by range-separation and care should be taken when using RS-functionals to predict the energies of association reactions. RS-functionals do behave much more as expected for energies that correspond to rearrangements of already existing complexes. We have not

scanned the full range of possible RS-functionals, and it may be that a suitable set of parameters can be found where a RS-functional provides superior performance provided that dispersion interactions are not important.

■ ASSOCIATED CONTENT

Supporting Information

Data that is averaged to give the results in Tables 1−5. This material is available free of charge via the Internet at http://pubs.acs.org/.

■ AUTHOR INFORMATION

Corresponding Author

*E-mail: ziegler@ucalgary.ca. Phone: (403)220 5368. Fax: (403)289 9488.

Notes

The authors declare no competing financial interest.

■ ACKNOWLEDGMENTS

T.Z. would like to thank the Canadian government for a Canada research chair in theoretical inorganic chemistry. We are grateful to NSERC for funding.

■ REFERENCES

(1) Becke, A. D. *J. Chem. Phys.* **1993**, *98*, 5648−5652.
(2) Becke, A. D. *J. Chem. Phys.* **1993**, *98*, 1372−1377.
(3) Stephens, P. J.; Devlin, F. J.; Chabalowski, C. F.; Frisch, M. J. *J. Phys. Chem.* **1994**, *98*, 11623−11627.
(4) Bylander, D. M.; Kleinman, L. *Phys. Rev. B* **1990**, *41*, 7868−7871.
(5) Savin, A. On degeneracy, near-degeneracy and density functional theory. In *Recent Developments and applications of modern density functional theory*; Seminario, J. M., Ed.; Elsevier: Amsterdam, 1995; pp 327−357.
(6) Savin, A.; Flad, H.-J. *Int. J. Quantum Chem.* **1995**, *56*, 327−332.
(7) Leininger, T.; Stoll, H.; Werner, H.-J.; Savin, A. *Chem. Phys. Lett.* **1997**, *275*, 151−160.
(8) Iikura, H.; Tsuneda, T.; Tanai, T.; Hirao, K. *J. Chem. Phys.* **2001**, *115*, 3540−3544.
(9) Tawada, Y.; Tsuneda, T.; Yanagisawa, S.; Yanai, T.; Hirao, K. *J. Chem. Phys.* **2004**, *120*, 8425−8433.
(10) Song, J.-W.; Tokura, S.; Sato, T.; Watson, M. A.; Hirao, K. *J. Chem. Phys.* **2007**, *127*, 154109.
(11) Song, J.-W.; Watson, M. A.; Hirao, K. *J. Chem. Phys.* **2009**, *131*, 144108.
(12) Heyd, J.; Scuseria, G. E.; Ernzerhof, M. *J. Chem. Phys.* **2003**, *118*, 8207−8215.
(13) Heyd, J.; Scuseria, G. E. *J. Chem. Phys.* **2004**, *121*, 1187−1192.
(14) Vydrov, O. A.; Scuseria, G. E. *J. Chem. Phys.* **2006**, *125*, 234109.
(15) Henderson, T. M.; Janesko, B. G.; Scuseria, G. E. *J. Phys. Chem. A* **2008**, *112*, 12530−12542.
(16) Yanai, T.; Tew, D. P.; Handy, N. C. *Chem. Phys. Lett.* **2004**, *393*, 51−57.
(17) Baer, R.; Neuhauser, D. *Phys. Rev. Lett.* **2005**, *94*, 043002.
(18) Chai, J.-D.; Head-Gordon, M. *J. Chem. Phys.* **2008**, *128*, 084106.
(19) Akinaga, Y.; Ten-no, S. *Chem. Phys. Lett.* **2008**, *462*, 348−351.
(20) Akinaga, Y.; Ten-no, S. *Int. J. Quantum Chem.* **2009**, *109*, 1905−1914.
(21) Peverati, R.; Truhlar, D. G. *J. Phys. Chem. Lett.* **2011**, *2*, 2810−2817.
(22) Henderson, T. M.; Izmaylov, A. F.; Scuseria, G. E.; Savin, A. *J. Chem. Phys.* **2007**, *127*, 221103.
(23) Gerber, I. C.; Angyan, J. G. *Chem. Phys. Lett.* **2005**, *415*, 100−105.
(24) Gerber, I. C.; Angyan, J. G. *Chem. Phys. Lett.* **2005**, *416*, 370−347.
(25) Peach, M. J.; Helgakar, T.; Sałek, P.; Keal, T. W.; Luntnæs, O. B.; Tozer, D. J.; Handy, N. C. *Phys. Chem. Chem. Phys.* **2006**, *8*, 558−562.
(26) Peach, M. J.; Cohen, A. J.; Tozer, D. J. *Phys. Chem. Chem. Phys.* **2006**, *8*, 4543−4549.
(27) Rohrdanz, M. A.; Herbert, J. M. *J. Chem. Phys.* **2008**, *129*, 034107.
(28) Rohrdanz, M. A.; Martins, K. M.; Herbert, J. M. *J. Chem. Phys.* **2009**, *130*, 054112.
(29) Vydrov, O. A.; Heyd, J.; Krukau, A. V.; Scuseria, G. E. *J. Chem. Phys.* **2006**, *125*, 074106.
(30) Song, J.-W.; Hirowasa, T.; Tsuneda, T.; Hirao, K. *J. Chem. Phys.* **2007**, *126*, 154105.
(31) Song, J.-W.; Peng, D.; Hirao, K. *J. Comput. Chem.* **2011**, *32*, 3269−3275.
(32) Mardirossian, N.; Parkhill, J. A.; Head-Gordon, M. *Phys. Chem. Chem. Phys.* **2011**, *13*, 19325−19337.
(33) Ziegler, T.; Autschbach, J. *Chem. Rev.* **2005**, *105*, 2695−2722.
(34) Cramer, C. J.; Truhlar, D. G. *Phys. Chem. Chem. Phys.* **2009**, *11*, 10757−10816.
(35) Yang, K.; Zheng, J.; Zhao, Y.; Truhlar, D. G. *J. Chem. Phys.* **2010**, *132*, 164117.
(36) Tognetti, V.; Cortona, P.; Adamo, C. *Int. J. Quantum Chem.* **2010**, *110*, 2320−2329.
(37) Hermet, J.; Cortona, P.; Adamo, C. *Chem. Phys. Lett.* **2012**, *519*−*520*, 145−149.
(38) Steinmann, S. N.; Wordrich, M. D.; Corminboeuf, C. *Theor. Chem. Acc.* **2010**, *127*, 429−442.
(39) Jiménex-Hoyos, C. A.; Janesko, B. G.; Scuseria, G. E. *J. Phys. Chem. A* **2009**, *113*, 11742−11749.
(40) Steinmetz, M.; Grimme, S., in preparation.
(41) Zhao, Y.; Truhlar, D. G. *Theor. Chim. Acta* **2008**, *120*, 215−241.
(42) Monenkov, Y.; Occhipinti, G.; Jensen, V. R. *J. Phys. Chem. A* **2009**, *113*, 11833−11844.
(43) Monenkov, Y.; Occhipinti, G.; Heyndrickx, W.; Jensen, V. R. *Eur. J. Inorg. Chem.* **2012**, 1507−1516.
(44) Sieffert, N.; Bühl, M. *Inorg. Chem.* **2009**, *48*, 4622−4624.
(45) Baerends, E. J.; et al. ADF2010, SCM. *Theoretical Chemistry*; Vrije Universiteit, Amsterdam, The Netherlands, 2010; http://www.scm.com (accessed Dec 2012).
(46) te Velde, G.; Bickelhaupt, F. M.; Baerends, E. J.; Fonseca Guerra, C.; van Gisbergen, S. J. A.; Snijders, J. G.; Ziegler, T. *J. Comput. Chem.* **2001**, *22*, 931−967.
(47) Baerends, E. J.; Ellis, D. E.; Ros, P. *Chem. Phys.* **1973**, *2*, 41−51.
(48) Versluis, L.; Ziegler, T. *J. Chem. Phys.* **1988**, *88*, 322−328.
(49) te Velde, G.; Baerends, E. J. *Phys. Rev. B* **1991**, *44*, 7888−7903.
(50) Fonseca Guerra, C.; Snijders, J. G.; te Velde, G.; Baerends, E. J. *Theor. Chim. Acta* **1998**, *99*, 391−403.
(51) Seth, M.; Ziegler, T. *J. Chem. Theory Comp.* **2012**, *8*, 901−907.
(52) Becke, A. D. *Phys. Rev. A* **1988**, *38*, 3098−3100.
(53) Perdew, J. P. *Phys. Rev. B* **1986**, *33*, 8822−8824.
(54) Lee, C.; Yang, W.; Parr, R. G. *Phys. Rev. B* **1988**, *37*, 785−789.
(55) Perdew, J. P.; Burke, K.; Ernzerhof, M. *Phys. Rev. Lett.* **1996**, *77*, 3865−3868.
(56) Tao, J.; Perdew, J. P.; Staroverov, V. N.; Scuseria, G. E. *Phys. Rev. Lett.* **2003**, *91*, 146401.
(57) Staroverov, V. N.; Scuseria, G. E.; Tao, J.; Perdew, J. P. *J. Chem. Phys.* **2003**, *119*, 12129.
(58) Zhao, Y.; Truhlar, D. G. *J. Chem. Phys.* **2006**, *125*, 194101.
(59) Ernzerhof, M.; Scuseria, G. *J. Chem. Phys.* **1999**, *110*, 5029−5036.
(60) Adamo, C.; Barone, V. *J. Chem. Phys.* **1999**, *110*, 6158−6170.
(61) te Velde, G.; Baerends, E. J. *J. Comput. Phys.* **1992**, *99*, 84.
(62) Wheeler, S. W.; Houk, K. N. *J. Chem. Theory Comp.* **2010**, *6*, 395−404.
(63) Franchini, M., personal communication.
(64) van Lenthe, E.; Baerends, E. J.; Snijders, J. G. *J. Chem. Phys.* **1993**, *99*, 4597−4610.

(65) van Lenthe, E.; Baerends, E. J.; Snijders, J. G. *J. Chem. Phys.* **1994**, *101*, 9783−9792.
(66) van Lenthe, E.; Ehlers, A.; Baerends, E. J. *J. Chem. Phys.* **1999**, *110*, 8943−8953.
(67) de Jong, G. T.; Solà, M.; Visscher, L.; Bickelhaupt, F. M. *J. Chem. Phys.* **2004**, *121*, 9982−9992.
(68) de Jong, G. T.; Diefenbach, A.; Bickelhaupt, F. M. *Chem. Phys.* **2005**, *313*, 261−270.
(69) de Jong, G. T.; Geerke, D. P.; Diefenbach, A.; Solà, M.; Bickelhaupt, F. M. *J. Comput. Chem.* **2005**, *26*, 1006−1020.
(70) de Jong, G. T.; Bickelhaupt, F. M. *J. Phys. Chem. A* **2005**, *109*, 9685−9699.
(71) de Jong, G. T.; Bickelhaupt, F. M. *J. Chem. Theory Comp.* **2006**, *2*, 322−335.
(72) Qssuintal, M. M.; Karlton, A.; Iron, M. A.; Boese, A. D.; Martin, J. M. L. *J. Phys. Chem. A* **2006**, *110*, 709−716.
(73) Zhao, Y.; Truhlar, D. G. *J. Chem. Theory Comp.* **2009**, *5*, 324−333.
(74) Jurečka, P.; Šponer, J.; Černȳ, J.; Hobza, P. *Phys. Chem. Chem. Phys.* **2006**, *8*, 1985−1993.
(75) Peverati, R.; Truhlar, D. G. *J. Phys. Chem. Lett.* **2012**, *3*, 117−127.
(76) Grimme, S.; Diedrich, C.; Korth, M. *Angew. Chem. Int. Ed.* **2006**, *45*, 625−629.
(77) Csonka, G. I.; Ruzsinszky, A.; Perdew, J. P.; Grimme, S. *J. Chem. Theory Comp.* **2008**, *4*, 888−891.
(78) Wodrich, M. D.; Corminbœuf, C.; von Ragué Schleyer, P. *Org. Lett.* **2006**, *8*, 3631−3634.
(79) Zhao, Y.; Truhlar, D. *Org. Lett.* **2006**, *8*, 5753−5755.
(80) Kamiya, M.; Tsuneda, T.; Hirao, K. *J. Chem. Phys.* **2002**, *117*, 6010−6015.
(81) Sato, T.; Tsuneda, T.; Hirao, K. *Mol. Phys.* **2005**, *103*, 1151−1164.
(82) Sato, T.; Tsuneda, T.; Hirao, K. *J. Chem. Phys.* **2007**, *126*, 234114.
(83) Kitaura, K.; Morokuma, K. *Int. J. Quantum Chem.* **2976**, *10*, 325−340.
(84) Ziegler, T.; Rauk, A. *Theor. Chim. Acta* **1977**, *46*, 1−10.
(85) Wigner, E.; Seitz, F. *Phys. Rev.* **1933**, *43*, 804−810.
(86) Wigner, E. *Phys. Rev.* **1934**, *46*, 1002−1011.
(87) Henderson, T. M.; Janesko, B. G.; Scuseria, G. E. *J. Chem. Phys.* **2008**, *128*, 194105.
(88) Truong, T. N.; Duncan, W. *J. Chem. Phys.* **1994**, *101*, 7408−7414.